Available online at www.sciencedirect.com
ScienceDirect
Journal of the European Ceramic Society 30 (2010) 2633–2642
www.elsevier.com/locate/jeurceramsoc

ZrB_2–SiC composites prepared by reactive pulsed electric current sintering

Songlin Ran, Omer Van der Biest, Jef Vleugels *

Department of Metallurgy and Materials Engineering (MTM), K.U.Leuven, Kasteelpark Arenberg 44, B-3001 Heverlee, Belgium

Received 4 February 2010; received in revised form 3 May 2010; accepted 16 May 2010
Available online 11 June 2010

Abstract

Fully densified ZrB_2–20 vol% SiC composites were produced by reactive pulsed electric current sintering (PECS) of a powder mixture containing ZrH_2, B, SiC and B_4C within a total thermal cycle time of only 50 min. During the combined synthesis and sintering process, the ZrH_2 powder decomposed gradually from ZrH_2 into ZrH_m and finally metal Zr that reacted with elemental B to form the ZrB_2 matrix. Reducing the ZrH_2 particle size by attritor milling significantly enhanced densification and allowed initiation of self-propagating high temperature synthesis (SHS) during PECS. The PECS grades exhibited a slightly textured structure, with ≤17% of the ZrB_2 grains oriented with their (0 0 1) planes perpendicular to the direction of pressure and DC current. Because of the ZrB_2 grain orientation, anisotropic mechanical properties were observed. Ceramics prepared from attritor milled powders and PECS with a pressure applied after 5 min upon reaching 1900 °C achieved excellent flexural strengths of 901–937 MPa. The hardness and fracture toughness were respectively 19.7–19.8 GPa and 4.0–4.7 MPa $m^{1/2}$ in the direction parallel and 20.2–21.3 GPa and 3.8–3.9 MPa $m^{1/2}$ in the direction perpendicular to the applied pressure.

Keywords: Reactive pulsed electric current sintering; Borides; SiC; Microstructures; Mechanical properties

1. Introduction

Zirconium diboride (ZrB_2) has an extremely high melting point of 3250 °C, high thermal conductivity of 60–140 W/m K, high hardness of 23 GPa, and strength exceeding 500 MPa, making it a very attractive material for use in high temperature applications.[1,2] In addition, the moderate density of 6.09 g cm^{-3} makes it an ideal candidate material for aerospace applications.[3] Moreover, ZrB_2 can be machined into complex components by electrical discharge machining (EDM) at relatively low cost due to its high electrical conductivity (10^8 S m^{-1}).[4] However, the low sinterability and poor oxidation resistance above 650 °C limits the application of monolithic ZrB_2 in air environments.[2] The addition of SiC as a secondary phase improves not only the densification but also the oxidation resistance, as well as the strength and fracture toughness of ZrB_2 ceramics.[5,6]

Literature reports on ZrB_2–SiC composites described different densification methods and a wide range of results.[4–14] ZrB_2–SiC composites with strengths above 1 GPa have been prepared by hot-pressing.[5,15] The unintentional incorporation of WC as contamination during the milling process however was reported to play an important role in improving the mechanical properties.[5] Oxygen impurities present on the starting powder surfaces were claimed to be the main obstacle for full densification and enhanced grain growth of ZrB_2.[2] The addition of SiC particles improves the densification due to the formation of an intergranular secondary phase and the removal of oxygen impurities by producing volatile gases.[2,6] The grain size, especially of the SiC phase, is the critical factor determining the strength of ZrB_2–SiC composites.[7,15] To minimize ZrB_2 and SiC grain growth, low temperatures and fine raw particles are essential in conventional pressureless sintering and hot pressing.

Reactive sintering was identified as an efficient route to prepare fully densified ZrB_2–SiC composites with fine grain sizes. The most commonly explored reactions are[4,12]:

$$2Zr + Si + B_4C \rightarrow 2ZrB_2 + SiC \quad (1)$$

$$2ZrH_2 + Si + B_4C \rightarrow 2ZrB_2 + SiC + 2H_2 \quad (2)$$

Both ZrB_2 and SiC are in situ synthesized in both reactions, but the volume content of SiC is confined to 25%. As an alternative route, reaction (3) has been used to densify ZrB_2–SiC composites at low temperatures.[9]

$$Zr + 2B + SiC \rightarrow ZrB_2 + SiC \quad (3)$$

* Corresponding author.
E-mail address: jozef.vleugels@mtm.kuleuven.be (J. Vleugels).

0955-2219/$ – see front matter © 2010 Elsevier Ltd. All rights reserved.
doi:10.1016/j.jeurceramsoc.2010.05.012

The resulting ZrB_2 grain size was as small as 1.5 ± 1.2 μm for the composite hot pressed at 1800 °C. However, in order to avoid igniting a self-propagating high-temperature synthesis (SHS) reaction, the thermal cycling process was longer than 20 h.[9] Furthermore, the use of cemented carbide (WC–Co) milling balls resulted in WC and Co contamination that assisted densification by liquid phase formation.[9]

Recently, HfB_2–SiC composites prepared by pulsed electric current sintering (PECS, also named SPS) were reported to retain their room temperature strength up to 1500 °C.[16] The mechanism is not clear, but it was believed that the electrical discharges during the PECS process broke down the non-conductive oxide impurities and facilitated their removal from the compact.[9] Therefore, PECS is thought to have potential advantages for the preparation of ultra high temperature ceramics (UHTCs) with good high-temperature properties.

The aim of this work was to process contamination-free ZrB_2–SiC composites within a short thermal cycle by reactive pulsed electric current sintering of ZrH_2, B, SiC and B_4C starting powder mixtures at 1900 °C and 50 MPa. The in situ reaction process was assessed as a function of the PECS processing parameters, as supported by in situ recorded temperature and gas evolution. The fully densified composites were characterized by means of X-ray diffraction (XRD) and scanning electron microscopy (SEM). The orientation mechanism of the ZrB_2 grains in the PECS composites and its effect on the mechanical properties are discussed.

2. Experimental procedure

2.1. Powder processing

Commercially available ZrH_2 (Grade G, Chemetall, Germany, average particle size = 5.5 μm), amorphous B (Grade I, H.C. Starck, Germany, BET = 14.7 m^2/g), SiC (β-SiC, Kaier Nanometer Technology Development Co. Ltd., China, BET = 70 m^2/g) and B_4C (HD 20, H.C. Starck, Germany, BET = 22.0–25.0 m^2/g) powders were used as starting materials.

The starting powders were prepared with a stoichiometry according to reaction (4), targeting 20 vol% SiC in the final ZrB_2–SiC composites. Due to the unavoidable oxidation in air, ZrO_2 and B_2O_3 impurities are present on the surfaces of the ZrH_2 and B starting powders. The use of ZrO_2 beads during milling also introduced some ZrO_2 into the powders. As reported earlier, B_2O_3 evaporates at elevated temperature but ZrO_2 must be removed by a chemical reaction.[17] Therefore, in this study, 1.0 wt% B_4C powder was added to all powder mixtures to react with and remove any ZrO_2 impurity according to reaction (5).[9]

$$ZrH_2(s) + 2B(s) + SiC(s) \rightarrow ZrB_2(s) + SiC(s) + H_2(g) \quad (4)$$

$$5B_4C(s) + 7ZrO_2(s) \rightarrow 7ZrB_2(s) + 3B_2O_3(g) + 5CO(g) \quad (5)$$

Two methods were used to prepare the precursor powders, i.e., ball mixing and attrition milling. In case of ball mixing, powders were mixed in ethanol for 24 h on a multidirectional mixer (Turbula T2A, WAB, Switzerland) using $\Phi = 5$ mm ZrO_2 milling beads (Grade TZ-3Y, Tosoh, Japan). Attrition milling (Dispermat CN 20, VMA-Getzmann GmbH, Germany) occurred in 2-propanol at 2000 rpm for 2–3 h using the same ZrO_2 milling beads. To prevent possible oxidation, attrition milling was conducted under an argon flow. After milling, the slurry was dried at 65 °C in a rotating evaporator and subsequently sieved with a 50 mesh sieve to minimize powder segregation and agglomeration. The resulting precursor powder mixtures were designated as BM24h (ball mixed 24 h), AM2h (attrition milled 2 h) and AM3h (attrition milled 3 h). To evaluate the effect of the milling method, ZrH_2 powders were ball mixed and attrition milled under the same conditions as for BM24h, AM2h and AM3h for reference purposes.

2.2. In situ synthesis and sintering

21 g of starting powder mixture was poured into a graphite die/punch set-up ($\Phi = 40$ mm) lined with a graphite paper. Details on the die/punch/powder assembly are provided elsewhere.[18] The synthesis and densification were conducted by PECS (Type HP D25/1, FCT Systeme, Rauenstein, Germany) in a dynamic vacuum. The temperature was automatically raised to 450 °C and then measured axially through the punch by an optical pyrometer, focused on the bottom of the upper punch about 2 mm from the top surface of the sample. Previous research on the temperature distribution during PECS indicated that the used temperature measurement set-up allowed a very accurate sample temperature control. The temperature difference between the centre of an electrically conductive TiN or insulating ZrO_2 disc and the controlling pyrometer was found to be <5 °C.[18] The samples were heated at 50 °C/min from 450 to 1900 °C. In all experiments, a minimum pressure of 4 MPa was applied to ensure constant contact of the electrodes with the die/punch/sample set-up and to allow the evacuation of volatile species from the set-up. For densification, a pressure of 50 MPa was applied. Two different pressure-loading cycles, cycle I and cycle II, were used. In cycle I, the pressure was applied after a dwell time of 5 min at 1900 °C. In cycle II, the pressure was applied as soon as reaching 1900 °C. For both cycles, the 50 MPa pressure was applied within 60 s. After dwelling at 1900 °C under 50 MPa for 5 min, the pressure was removed gradually within 5 min while the composite was rapidly cooled to about 600 °C. The obtained bulk materials were designated according to their original powders and sintering cycles. For example, the material prepared from AM3h powders using cycle I was designated as AM3h-I. In this study, BM24h-I, AM2h-I, AM2h-II, AM3h-I and AM3h-II grades were investigated.

2.3. Characterization

Differential thermal analysis (DTA, SDT Q600, TA Instruments, Newcastle, USA) was conducted in Ar with a heating rate of 10 °C/min. After sandblasting and grinding to remove the surface impurities, the bulk density was determined by the Archimedes method in ethanol. The phase composition was

characterized by X-ray diffraction (XRD, 3003 TT, Seifert, Ahrensburg, Germany) using Cu Kα radiation with a scanning rate of 0.5 °/min. The morphology of the powders and constituent phases in the PECS grades were examined by scanning electron microscopy (SEM, XL30-FEG, FEI, Eindhoven, The Netherlands).

The elastic modulus was measured on a ground disk using the impulse excitation technique (IET, Grindo-Sonic, J.W. Lemmens N.V., Leuven, Belgium). Vickers hardness was measured on a hardness tester (Model FV-700, Future-Tech Corp., Tokyo, Japan) with a load of 5 kg and a dwell time of 10 s. The indentation toughness was evaluated from the radial crack pattern accompanying the Vickers indentations and calculated according to the Anstis equation.[19] The reported values are the mean and standard deviations from 5 indentations. Flexural strength was measured on ground rectangular bars (2 mm × 1.5 mm × 25 mm) using a three-point bending test (Instron 4467, Instron, Norwood, MA) with a span of 20 mm and a loading speed of 0.1 mm/min. The reported values are the mean and standard deviations of 7 bending bars.

3. Results and discussion

3.1. Reaction studies and powder characterization

In order to understand the reaction between ZrH_2 and amorphous B, a homogeneous 24 h ball mixed powder mixture with a ZrH_2/B molar ratio of 1/2 was dry pressed into a disk and heated at 700 °C in vacuum for 1 h. Analysis of the XRD patterns (Fig. 1) revealed that the product was metal Zr with a small amount of ZrB_2, implying that ZrH_2 first decomposed into metal Zr before reacting with B to form ZrB_2. Therefore, it can be concluded that the reaction between ZrH_2 and B is basically the same as the reaction of Zr and B with a superimposed dehydrogenation of ZrH_2.

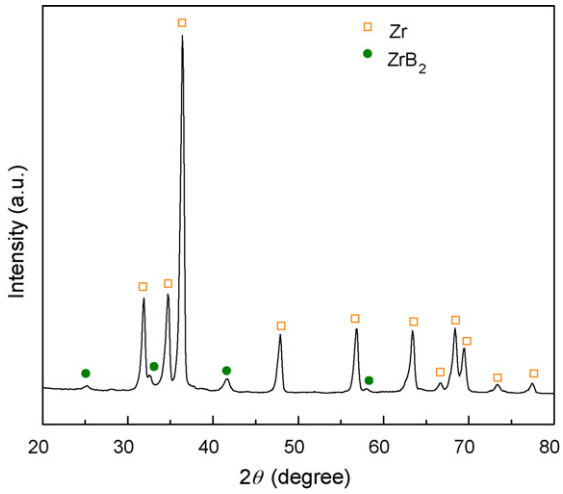

Fig. 1. XRD pattern of a ZrH_2–B powder compact after heating in vacuum for 1 h at 700 °C.

When metal Zr reacts with B, the B dissolves and diffuses into the metal Zr to form ZrB_2.[20] Therefore, the size and shape of the ZrB_2 product will be strongly influenced by the Zr starting powder. Since metal Zr is ductile and difficult to be milled down to small particle sizes, the use of brittle ZrH_2 is thought to be a suitable alternative to easily obtain small starting powders. Metal Zr is also considered to be more prone to self-ignition or oxidation in air compared to ZrH_2. Moreover, the particle size can be further decreased by the decomposition of ZrH_2. In the present study, submicrometer sized ZrH_2 powder was obtained by attrition milling commercial ZrH_2 powders. SEM image analysis of pristine, ball milled and attrition milled ZrH_2 powders, as illustrated in Fig. 2, revealed a substantial particle size reduction upon attrition milling. The average particle size of the pristine ZrH_2 powder is 5.5 ± 3.2 μm, as measured by the linear intercept method on 150 randomly selected particles on SEM images, with the largest particles up to 15.5 μm (Fig. 2(a)).

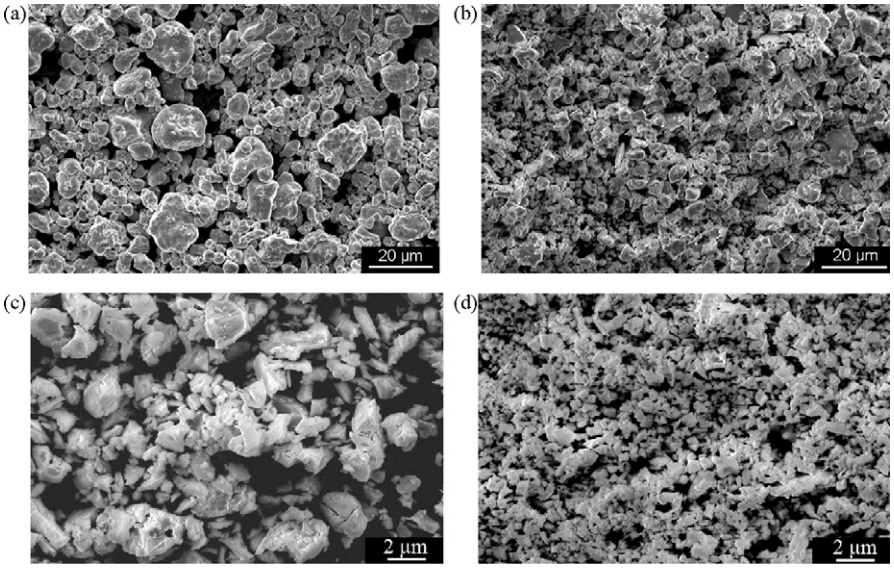

Fig. 2. Morphology of pristine (a), ball mixed (b) and 2 h (c) and 3 h (d) attrition milled ZrH_2 powders.

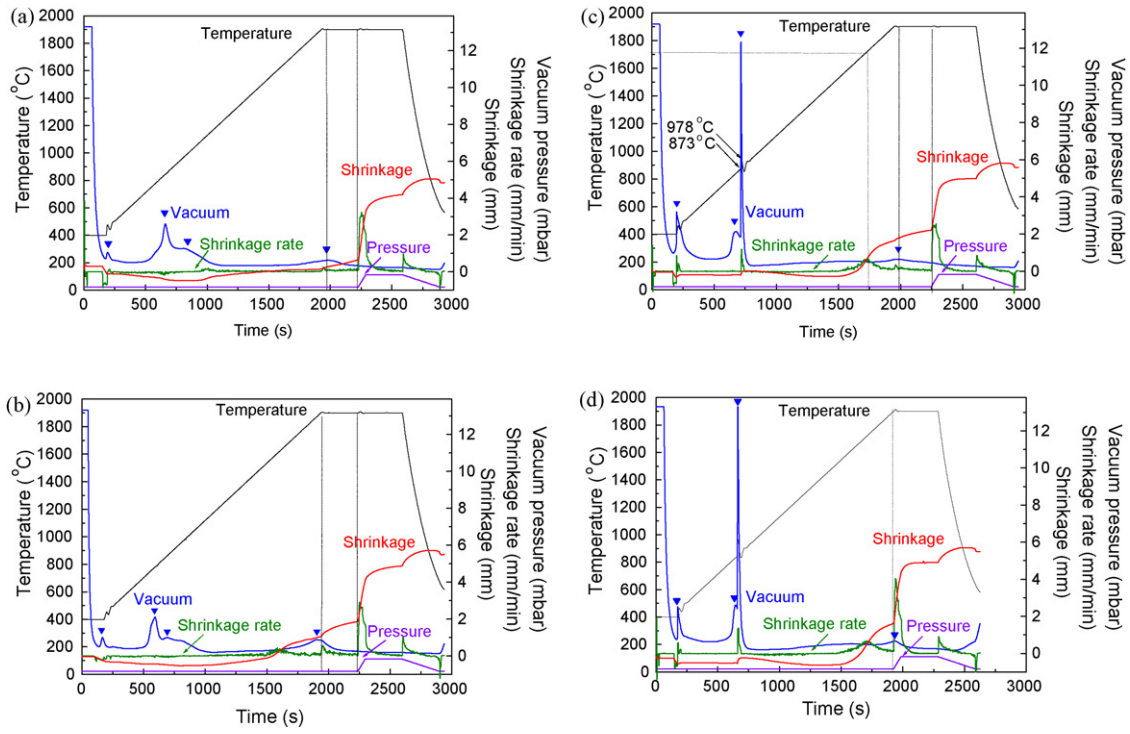

Fig. 3. PECS data of BM24h-I (a), AM2h-I (b), AM3h-I (c) and AM3h-II (d).

During ball mixing, some large particles were reduced in size but the average particle size, 4.0 ± 1.8 μm, only slightly changed (Fig. 2(b)). After attrition milling however, the average particle size reduced to 1.3 ± 0.8 μm and 0.5 ± 0.2 μm after 2 (Fig. 2(c)) and 3 h (Fig. 2(d)) milling respectively. The particle morphology also changed from spherical to irregular for attrition milled powders. As a result, the attritor milled ZrH_2 powders are expected to have a higher reactivity than the pristine or ball mixed powders.

3.2. *In situ synthesis and sintering*

In this study, a heating rate of 50 °C/min was used to in situ synthesize and sinter ZrH_2–B–SiC–B_4C powders in one step using PECS. During the PECS process, the changes in temperature, pressure, vacuum level, shrinkage and shrinkage rate were recorded to allow elucidating the reactive synthesis and densification process. Typical PECS data for BM24h-I, AM2h-I, AM3h-I and AM3h-II are summarized in Fig. 3.

After uncontrolled fast heating to the onset reading point of the pyrometer, the temperature was monitored and controlled by an optical pyrometer above 450 °C. The temperature fluctuation between 400 and 500 °C is due to the transition of uncontrolled rapid heating to controlled thermal cycling. As shown in Fig. 3(a) and (b), the actual temperature curves above 500 °C for BM24h-I and AM2h-I increase linear with time, as pre-programmed at 50 °C/min. For the AM3 h powders however, the temperature increases sharply from 873 to 978 °C within a second and returns to the programmed temperature rate with an adjusting oscillation, as illustrated in Fig. 3(c) and (d). This means that an abrupt exothermic reaction has occurred. Since the reaction between metal Zr and B is reported to be highly exothermic with an adiabatic temperature of 3050 °C,[9] a self-propagating high-temperature synthesis (SHS) reaction can be ignited by a current pulse.[21,22]

During PECS of the AM3h powder, the SHS reaction was ignited at 873 °C during heating at 50 °C/min, whereas this reaction was not ignited for the BM24h and AM2h grades. Since the only difference amongst these powders is their particle size, it is clear that finer powders have a higher reactivity and easier initiate a SHS reaction, what has also been reported for reactive hot pressing of Zr–Si–B_4C powders.[23] From the PECS experiments and particle size of the powder grades, it can be concluded that the critical particle size of ZrH_2 for ignition SHS reaction under the applied experimental conditions was between 1.3 and 0.5 μm.

Just like the temperature curves, the vacuum levels during thermal cycling of the three powders are also different. 4 peaks can be differentiated in the vacuum curves of all samples, as indicated by the filled symbols in Fig. 3. The first peak below 500 °C is due to the degassing and dehydration of the starting powders, and started upon applying the current. The second and third peaks between 600 and 1000 °C correlate to the reaction of ZrH_2 and B. The fourth peak at 1900 °C reflects the release of B_2O_3 (g) and CO (g) due to the proceeding of reaction (5) and B_2O_3 evaporation.

DTA analysis of pristine ZrH_2 and AM3 h powders presents two endothermic peaks, as shown in Fig. 4, which reveals that the dehydrogenation of ZrH_2 to metal Zr involves a two-step process. Since a similar result was reported for TiH_2,[24] we can conclude that the dehydrogenation of ZrH_2 is a gradual process with the following sequence: $ZrH_2 \rightarrow ZrH_m \rightarrow Zr$ and therefore, the second vacuum peak in Fig. 3 can be attributed to

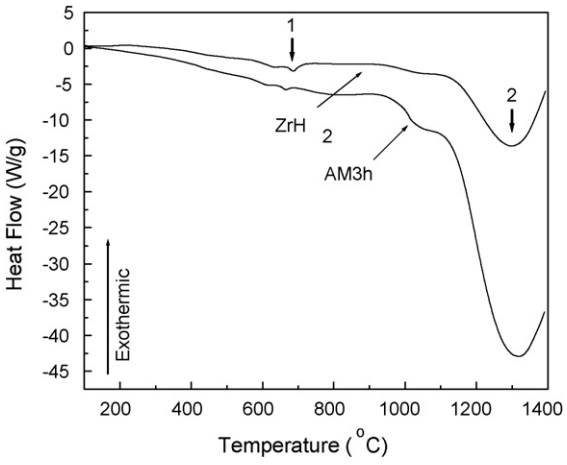

Fig. 4. Differential thermal analysis data for pristine ZrH_2 and AM3 h powders.

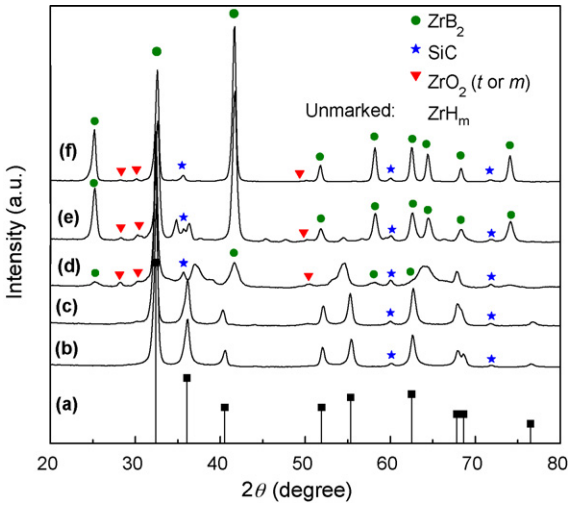

Fig. 5. JCPDS card no. 17-0314 (a) and XRD patterns of the AM3h powder before (b) and after heating at 600 (c), 850 (d), 1000 (e) and 1450 °C (f).

the hydrogen release during the first step of the dehydrogenation process from ZrH_2 to ZrH_m. Due to the different heating rate, the corresponding temperature for the first dehydrogenation process during PECS is about 100 °C higher than in DTA (see Figs. 3 and 4), what was also reported for the PECS decomposition of MgH_2.[25]

The main difference amongst the three powders is the third vacuum drop peak, which is low and broad for the BM24h and AM2h powders and high and sharp for AM3h. As discussed above, the SHS reaction was ignited at 873 °C only for attrition milled AM3h powder. The intensive SHS reaction was completed within a few seconds and the produced gas was released in a very short time. Consequently, a strong vacuum drop is noticed at the same temperature as the initiating point for the SHS reaction. In the absence of the SHS reaction, the second step of the dehydrogenation from ZrH_m to Zr shifts the maximum gas release to a higher temperature and also spreads the hydrogen release in time.

To assess the reaction process, the PECS cycles were stopped at predefined temperatures. XRD patterns of the AM3h powder treated at 600, 850, 1000 and 1450 °C, as well as the milled starting powder, are compared in Fig. 5. The JCPDS 17-0314 card is used as reference for ZrH_2. Since the B source is amorphous, only ZrH_2 and SiC phases can be detected in Fig. 5(b). The ZrH_2 peaks in the AM3h powder coincide with those of the reference, indicating there was no reaction during the attrition milling process. The powder treated at 600 °C has a similar XRD pattern (Fig. 5(c)) as the milled powder. When heated at 850 °C, a substantial ZrH_2 peak shift is notable (Fig. 5(d)) and the appearance of ZrB_2 peaks indicates that a fraction of the ZrH_2 powder was totally dehydrogenated to form metal Zr which reacted with elemental B. The second vacuum drop during PECS was observed between 600 and 850 °C, implying that a substantial amount of hydrogen was released from the compact. Therefore, the XRD peak shifts of the ZrH_2 phase can be attributed to the partial dehydrogenation of ZrH_2. The partial removal of hydrogen from the ZrH_2 influences the unit cell parameters.

With increasing temperature, more and more ZrH_2 completely dehydrogenated while the strong exothermal reaction between Zr and B made the reaction self-sustaining. The dehydrogenation of ZrH_2 and the formation of ZrB_2 proceeded together in a short period of time. When heating to 1000 °C, mainly ZrB_2 is present as shown in Fig. 5(e). Some traces of partial dehydrogenated ZrH_2 or metal Zr can still be found implying that the reaction was not completed. The residual ZrH_2 or Zr was converted into ZrB_2 as the temperature was increased to 1450 °C, as revealed in Fig. 5(f).

During PECS, the pressure was kept constant at 4 MPa to ensure good contact of the electrodes with the die/punch/sample set-up before increasing the pressure to 50 MPa at 1900 °C. Because of the applied minimum pressure, the punch displacement is very sensitive to the volume change of the powder compact. As shown in Fig. 3, the shrinkage/expansion and shrinkage rate curves are powder grade specific. For BM24h-I, the material initially expands up to about 1000 °C and then shrinks with increasing temperature. The total shrinkage below 1900 °C is limited. For AM3h-I and AM3h-II, an abrupt limited shrinkage is measured around the SHS ignition temperature. Since the reaction was nearly complete after the SHS reaction, the ZrB_2 and SiC powder compact expands first with increasing temperature and the onset of densification is found at 1540 °C. The shrinkage rates between 1540 and 1900 °C are much higher than for BM24h. The shrinkage curve for AM2h-I is similar to that of BM24h-I below but more like AM3h-I above 1500 °C.

Prior to increasing the pressure, the shrinkage for AM3h-I was 2.21 mm, i.e., more than 3 times higher than for BM24h-I. For all material grades, the shrinkage curves increase sharply upon increasing the pressure. After holding at 1900 °C under 50 MPa for 5 min, the shrinkage curve kept increasing for BM24h-I while reaching a stable level for AM2h-I and AM3h-I. This implies that the ball mixed powders were not yet fully densified and the attrition milled powders achieved near complete densification, which is confirmed by a density of 5.03, 5.61 and 5.62 g cm^{-3} for BM24h-I, AM2h-I and AM3h-I respectively.

As discussed above, the temperature sharply increased and an excessive amount of H_2 gas was released immediately after the SHS reaction was ignited, frequently resulting in graphite die explosion. In order to reduce the risk on tool destruction, 8

notches with depth below 0.5 mm were made along the length of the punch walls to enhance gas release from the powder compact in all further experiments. In this context, PECS of AM2h-I powder, avoiding initiation of the SHS reaction, is preferred over sintering of AM3h-I.

3.3. Removal of oxide impurities

Oxygen impurities in the starting powders, especially ZrO_2 and B_2O_3, have been shown to promote ZrB_2 coarsening.[26] B_4C was used to remove ZrO_2 during traditional pressureless sintering or hot pressing according to reaction (5).[9,26] Thermodynamic calculations and experimental results confirmed both ZrO_2 and B_2O_3 could be removed at temperatures as low as 1450 °C in vacuum by reaction and volatilization.[9,26,27] However, in the case of PECS, the result is different. Our previous research on B_4C–TiB_2 revealed that the volatilisation of B_2O_3 was significantly delayed during PECS due to the fact that the powder compact is relatively isolated from the furnace atmosphere.[28] The onset of gas release was found to occur around 1750 °C for B_4C–TiB_2.[28] This temperature is comparable to the onset temperature for the fourth peak in the vacuum curves in Fig. 3.

In order to confirm the delay of reaction (5) during PECS, AM3h powders were sintered according to cycle I and cycle II. The experimental data for AM3h-I and AM3h-II are compared in Fig. 3(c) and (d). The data for both cycles are similar below 1900 °C, illustrating the reproducibility of the experiments. When reaching 1750 °C, the vacuum curve begins to rise and reaches a maximum at 1900 °C, implying a release of gas. Before applying an increased pressure, the vacuum level in loading cycle I was restored, implying reaction (5) had completed and all B_2O_3 was evaporated. In loading cycle II however, the vacuum level is still at the maximum point and it is the increased applied pressure on the compact that makes the vacuum curve drop. The applied higher pressure can easily seal off the actual powder compact from the surrounding vacuum vessel. In this way, B_2O_3 vapour was entrapped in the sintering powder compact, which prohibited reaction (5) to reach completion. As a result, ZrO_2 could not be completely removed in cycle II. XRD analysis confirms that there was still some residual ZrO_2 in the AM3h-II sample, as shown in Fig. 6(b).

The presence of ZrO_2 also inhibited the densification of the ZrB_2–SiC composites, as illustrated by the lower density of 5.53 g cm^{-3} for cycle II compared to 5.62 g cm^{-3} for cycle I.

Traces of ZrC were found for AM3h-I but not for AM3h-II, as shown in Fig. 6, indicating some ZrC formed during the low pressure dwell period at 1900 °C. A possible explanation is that the CO gas produced by reaction (5) or C from the punch/die set-up reduced ZrO_2 to metal Zr, which reacted with B_4C or C to form ZrC. Due to the lower amount of ZrO_2 contamination during attrition milling of AM2h compared to the AM3h powder grade, no ZrC was found in the densified AM2h-I grade.

3.4. Orientation of ZrB_2 grains

Fig. 6 indicates that the peaks at 25.2° (2θ) have a higher intensity than those at 32.6°, which are different from the reference ZrB_2 pattern (JCPDS 34-0423 shown in Fig. 7(a)). This implies that the hexagonal ZrB_2 grains have grown in a preferred direction. XRD patterns of a top (TS) and side surface (SS), respectively perpendicular and parallel to the pressing direction as well as the current flow direction, are compared in Fig. 7. It is clear that the relative intensity of the (0 0 1) plane is much higher than that of the (1 0 0) plane and comparable to the (1 0 1) plane on the TS surface (Fig. 7(b)), whereas the (1 0 0) plane is the most intense on the SS surface (Fig. 7(c)). (0 0 1) planes are perpendicular to the *c*-axis of the grains, therefore ZrB_2 grains grew with an aligned *c*-axis. Similar results have been reported recently on reactive hot-pressed ZrB_2–$MoSi_2$ composites.[29]

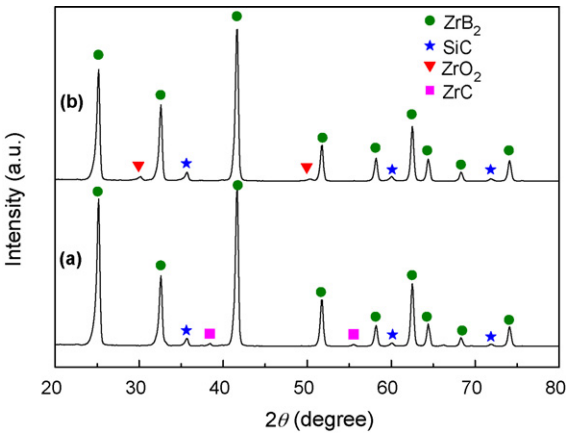

Fig. 6. XRD patterns of AM3h-I (a) and AM3h-II (b).

The degree of orientation can be quantified[30,31] by the Lotgering orientation factor (*f*), which was measured to be 0.17 for AM3h-I. In reactive hot-pressed of ZrB_2–$MoSi_2$ composites, an orientation factor of 0.16 for ZrB_2 was claimed to enhance the fracture toughness from 2.3–2.8 to 4.9 MPa m$^{1/2}$.[29] In this study, the orientation of ZrB_2 grains also affected the mechanical properties considerably, as discussed below.

To assess the influence of different factors on the orientation, the $\mathbf{I}_{(001)}/\mathbf{I}_{(100)}$ intensity ratios obtained from XRD patterns of TS surfaces of different samples are compared in Fig. 8. The

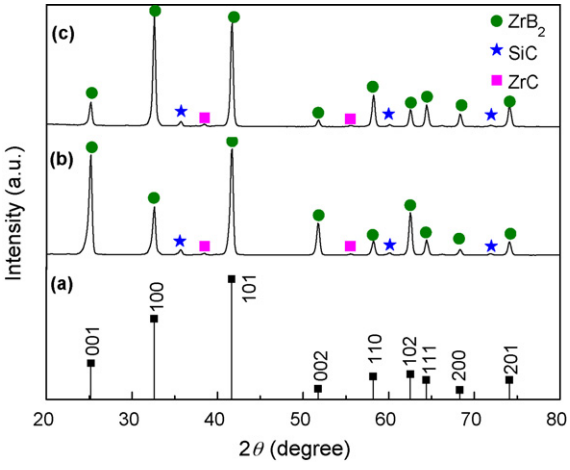

Fig. 7. ZrB_2 JCPDS 35-0741 reference (a) and XRD patterns of TS (b) and SS (c) surface of AM3h-I.

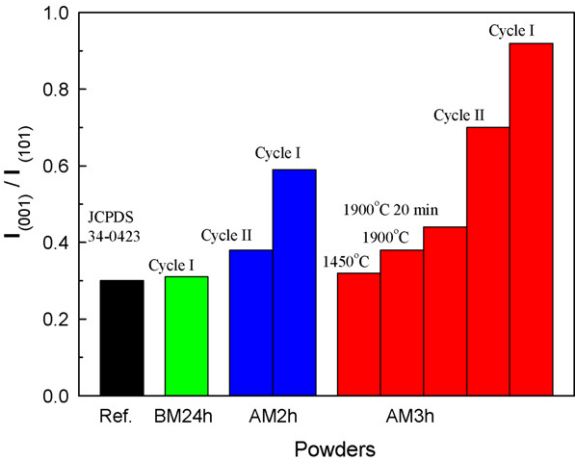

Fig. 8. XRD $\mathbf{I}_{(001)}/\mathbf{I}_{(100)}$ intensity ratios of surfaces perpendicular to the pressing direction of different ceramic grades.

ratio for BM24h-I (0.31) is similar as for JCPDS 34-0423 (0.30), implying there is no preferred ZrB_2 grain orientation in this ceramic. For AM2h powders, the ratio is 0.59 for cycle I and 0.38 for cycle II, respectively. PECS AM3h powders have the highest ratios, i.e., 0.92 for cycle I and 0.70 for cycle II.

Additional PECS cycles on AM3h powder were stopped at 1450 °C, at 1900 °C without dwell period and at 1900 °C with a dwell period of 20 min at minimum pressure. The peak intensity ratios measured on the obtained ceramics are included in Fig. 8. No preferred orientation of the AM3h starting powders was observed after PECS at 1450 °C, whereas a clear texture was measured when PECS at 1900 °C. Holding at 1900 °C for 20 min slightly enhanced the degree of orientation. In addition, the peak intensity ratios for cycle I are much higher than for cycle II.

Based on the above results and literature reports,[32–34] the orientation of ZrB_2 grains can be attributed to an anisotropic Ostwald ripening process under pressure. The crystal structure of ZrB_2 is primitive hexagonal with anisotropy in the *a*-($a = 0.3168$ nm) and *c*-axis ($c = 0.3530$ nm).[1] It is possible for ZrB_2 powders to grow in a certain direction due to anisotropic interfacial energies. It is well know that a liquid phase is the key factor in Ostwald ripening. In the present study, B_2O_3 and SiO_2 are the potential liquid phases, which originate from the B, B_4C and SiC starting powder particle surfaces. During PECS, there is always a minimum contact pressure, 4 MPa in the present case, on the powders that can promote preferential growth of ZrB_2 particles with respect to the pressure direction. Although B_2O_3 begins to evaporate at 1750 °C, SiO_2 glass originating from the SiC starting powder can serve as a liquid phase at higher temperature.

According to the Ostwald ripening mechanism, the smallest grains will dissolve in the liquid and the appropriate constituents diffuse towards the surface of larger grains to re-precipitate.[33] The grains are initially randomly oriented, but some large grains with certain orientation tend to grow during sintering at the cost of smaller grains.[34] Since the liquid phases in the current study originate from the oxide layer on the starting powders, the amount is limited. Therefore, only those grades with very fine particles, i.e., the attritor milled powder based grades, are susceptible to this mechanism. This explains why the attrition milled powders (AM3h and AM2h) exhibited a tendency to orientation whereas the ball mixed powders BM24h showed no preferred orientation. For the same reason, increasing the temperature from 1450 to 1900 °C for AM3h powders could only slightly improve the orientation. Upon applying a higher pressure of 50 MPa, the distance between the particles is narrowed and the transportation of constituents through the liquid phase becomes more effective. As a result, the preferred orientation of ZrB_2 grains increased significantly.

As discussed above, reaction (5) could proceed to completion after a 5 min dwell time at 1900 °C before increasing the pressure (cycle I). Completion of this reaction brings more liquid B_2O_3 into the system, which benefits ZrB_2 grain orientation. Moreover, the dwell period provides more templated ZrB_2 grains that favour anisotropic grain growth during densification.[32] Due to this additional amount of templated grains, the orientations in the ceramics prepared according to loading cycle I are higher than for cycle II, as shown in Fig. 8.

3.5. Microstructures

Recently, the authors reported on the preparation of textured monolithic TiB_2 ceramics by in situ PECS synthesis.[35] The TiB_2 with a Lotgering orientation factor of 0.66 ((0 0 1) plane) had a clear microstructural anisotropy.[35] In this study, the difference in ZrB_2 grain morphology perpendicular and parallel to the pressure direction is less pronounced, as illustrated in Fig. 9, due to the limited orientation factor of ≤0.17. Dark SiC grains can be clearly differentiated from the grey ZrB_2 matrix. A small amount of dispersed white ZrC grains are found in Fig. 9(d), which is in agreement with the XRD analysis (Fig. 7). The ZrB_2 grain size for AM3h-I (with ignition) was larger than for AM2h-I (without ignition), despite the finer starting powder (Fig. 2(c) and (d)). The average ZrB_2 grain size on the TS and SS surfaces is 2.3 ± 0.5 and 2.7 ± 0.4 μm for AM2h-I and 4.0 ± 0.3 and 4.1 ± 0.9 μm for AM3h-I respectively, as measured by the linear intercept method on 50 grains.[36] The coarser grain size of AM3h-I can be explained by its higher orientation degree (Fig. 8) with the formation of some elongated ZrB_2 grains (Fig. 9(d)) due to the mechanism discussed above. A more pronounced orientated of ZrB_2 grains with high aspect ratio is likely to be obtained by generating more liquid phase during densification.

3.6. Mechanical properties

The mechanical properties of the ceramics are summarized in Table 1. The theoretical density, as calculated from the rule of mixtures for a ZrB_2–20 vol% SiC composite, is 5.51 g cm^{-3}. The higher values obtained for the AM2h-I and AM3h-I can be explained by the ZrO_2 impurity introduced during attritor milling that was converted to ZrB_2 according to reaction (5) with the concomitant formation of ZrC (6.74 g cm^{-3}), with a higher density than ZrB_2 (6.09 g cm^{-3}), when applying PECS cycle I (Fig. 6). Due to the comparable density of ZrO_2, remaining when

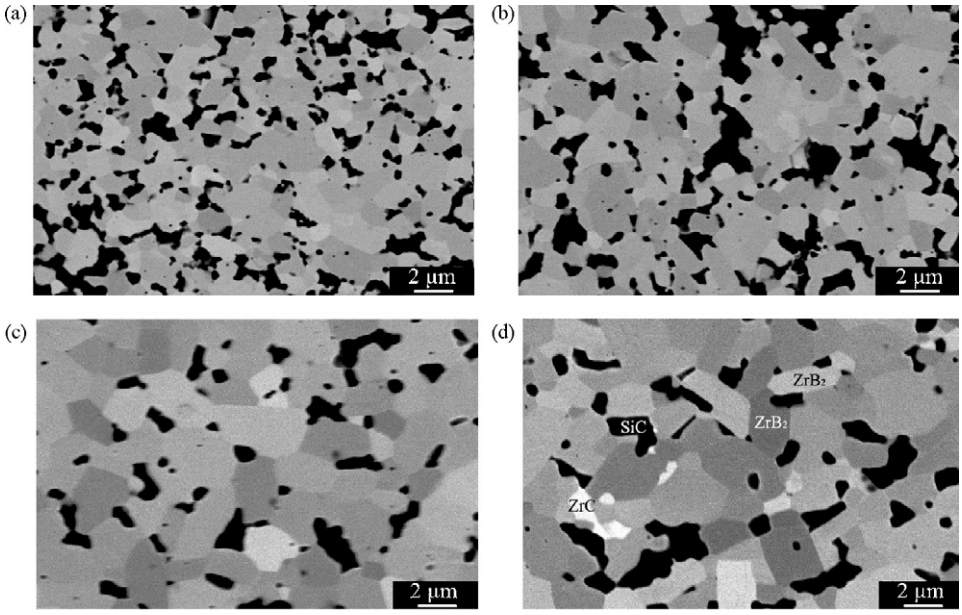

Fig. 9. Backscattered electron micrographs of polished TS (a, c) and SS (b, d) surfaces of AM2h-I (a, b) and AM3h-I (c, d).

applying PECS cycle II (Fig. 6), and ZrB_2, ceramic AM3h-II can be considered to be fully dense whereas AM2h-II and BM24-I contain residual porosity.

The elastic modulus of the ceramic grade correlates well with the density. Ceramics AM3h-I, AM2h-I and AM3h-II are fully dense and have high *E*-moduli. The *E*-modulus of AM2h-I is slightly higher than for AM3h-I due to the slightly lower ZrC content resulting from the shorter attritor milling time. Research on ZrC–ZrB_2–SiC composites indicated that the elastic modulus indeed decreased with increasing ZrC addition.[37]

When the tensile surfaces were perpendicular to the direction of pressure and DC current during sintering, the tested 3-point flexural strengths of AM2h-I and AM3h-I are 901 ± 115 and 937 ± 84 MPa, respectively. These values are very high, even when compared to hot-pressed ZrB_2-SiC composites with WC addition.[4–7,9] In addition to a combination of full densification and the use of a nanometric SiC grain growth inhibitor, the excellent flexural strength is respectively attributed to the reduced ZrB_2 grain size for AM2h-I and the formation of elongated ZrB_2 grains and concomitant toughness improvement for AM3h-I during the reactive PECS process. The lower strengths for AM2h-II and AM3h-II are due to the residual porosity and entrapped B_2O_3 phase, respectively.

Table 1
Mechanical properties of ZrB_2–SiC composites.

Material grade	BM24-I	AM2h-I	AM2h-II	AM3h-I	AM3h-II
Density ($g\,cm^{-3}$)	5.03	5.61	5.40	5.62	5.53
E-modulus (GPa)	–	510 ± 2	461 ± 3	505 ± 3	494 ± 4
Flexural strength (MPa)					
TS	–	901 ± 115	685 ± 93	937 ± 84	700 ± 120
Hardness (GPa)					
TS	–	20.2 ± 0.6	18.5 ± 0.3	21.3 ± 0.7	19.9 ± 1.0
SS	–	19.8 ± 0.5	19.2 ± 0.3	19.7 ± 0.7	20.2 ± 0.2
Fracture toughness ($MPa\,m^{1/2}$)					
TS	–	3.8 ± 0.1	3.4 ± 0.1	3.9 ± 0.3	3.6 ± 0.2
SS	–	4.0 ± 0.3	3.5 ± 0.2	4.7 ± 0.3	3.9 ± 0.4

In the less textured ceramic grades, the hardness and fracture toughness in the SS surfaces are nearly the same as in the TS surfaces, when taking into account the standard deviation on the measurements. For the most textured ceramic AM3h-I however, the hardness and fracture toughness on the TS surface is 1.6 GPa higher and 0.8 $MPa\,m^{1/2}$ lower than on the SS surface, respectively. The hardness in highly textured ZrB_2 and ZrB_2–SiC ceramics with a Lotgering orientation factor of the (0 0 1) plane of 0.95, prepared by strong magnetic field alignment (SMFA) and PECS densification, was recently reported to be about 15% higher on the SS than on the TS surface.[31] Although the materials prepared by SMFA were nearly completely textured, there was no morphology difference between the TS and SS surfaces and the hardness difference was related to a different residual stress level caused by the anisotropic coefficient of thermal expansion along the ZrB_2 *a*- and *c*-axis directions in both directions.[31] In this study however, the limited orientation of the ZrB_2 phase was accompanied by the formation of elongated ZrB_2 grains, which may cause a different porosity distribution, phase composition as well as residual stress level in different directions.

The higher fracture toughness of ceramic AM3h-I on the SS compared to the TS surface can be attributed to the presence of higher aspect ratio ZrB_2 grains in the SS plane. Amongst the active toughening mechanisms observed are crack deflection and crack bridging, as shown in Fig. 10. The measured values, ranging from 3.4 to 4.7 $MPa\,m^{1/2}$ are higher or comparable than the reported values measured according to the same method.[4,9,13] Similar ceramics prepared by reactive hot pressing of Zr–B–SiC powder mixtures however were reported to have a lower fracture toughness, ranging from 1.7 to 2.1 $MPa\,m^{1/2}$.[9]

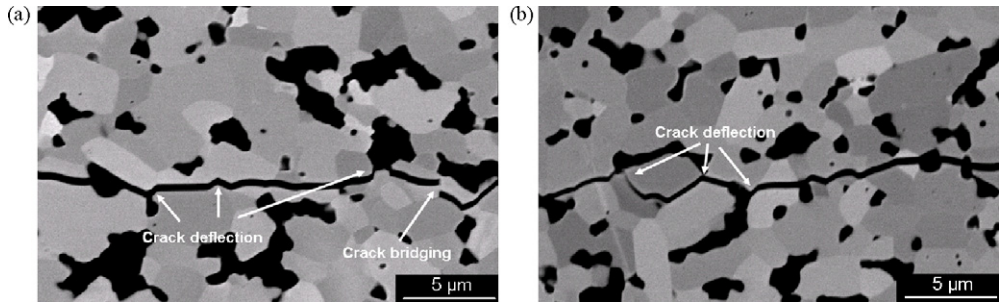

Fig. 10. Crack propagation in the SS surface of AM3h-I.

4. Conclusions

ZrB_2–20 vol% SiC composites were in situ synthesized and densified by pulsed electric current sintering (PECS) of a ZrH_2, B, SiC and B_4C starting powder mixture within a total thermal cycle time of only 50 min. Analysis of the PECS parameters revealed that the ZrH_2 powder gradually dehydrogenates from ZrH_2 over ZrH_m to Zr. When the ZrH_2 particle size was fine enough, as realized by attritor milling for 3 h, a SHS reaction between metal Zr and elemental B could be ignited during PECS. The presence of the SHS reaction significantly enhanced densification but also increased the risk of tool destruction. Adjusting the attritor milling time to 2 h allowed to avoid initiating the SHS reaction and to obtain full densification without the risk of die fracture.

The particle size reduction of the ZrH_2 starting powder was found to be a crucial factor in enhancing densification. Moreover, the loading cycle turned out to be even more important. PECS at 1900 °C for 5 min before increasing the pressure to 50 MPa was essential to remove oxygen impurities and obtain full densification under both SHS initiated and absent conditions.

The prepared ZrB_2–SiC composites showed limited ZrB_2 grain orientation, with the (0 0 1) planes perpendicular to the direction of pressure and DC current. The orientation mechanism was explained according to the Ostwald ripening theory. The presence of liquid phases, attrition milled starting powder and high pressure were crucial parameters for preferential ZrB_2 grain growth.

The 3-point flexural strength of the fully densified ceramics ranged from 901 to 937 MPa, in combination with a fracture toughness of 3.8–4.7 MPa $m^{1/2}$ and Vickers hardness of 19.7–21.3 GPa. Due to the orientation of the ZrB_2 grains, a small anisotropy in hardness and toughness was measured in the ceramic grade with the highest texture. The hardness and toughness in the direction perpendicular to the pressure direction was respectively 1.6 GPa higher and 0.8 MPa $m^{1/2}$ lower than in the parallel direction.

Acknowledgements

This work was supported by the Research Fund of K.U.Leuven under project GOA/08/007, the Flanders-China bilateral project BIL 07/06 and the Fund for Scientific Research Flanders (FWO) under project no. G.0305.07.

References

1. Fahrenholtz WG, Hilmas GE, Talmy IG, Zaykoski JA. Refractory diborides of zirconium and hafnium. *J Am Ceram Soc* 2007;**90**: 1347–64.
2. Guo S-Q. Densification of ZrB_2-based composites and their mechanical and physical properties: a review. *J Eur Ceram Soc* 2009;**29**: 995–1011.
3. Mitra R, Upender S, Mallik M, Chakraborty S, Ray KK. Mechanical, thermal and oxidation behaviour of zirconium diboride based ultra-high temperature ceramic composites. *Key Eng Mater* 2009;**395**:55–68.
4. Zimmermann JW, Hilmas GE, Fahrenholtz WG, Monteverde F, Bellosi A. Fabrication and properties of reactively hot pressed ZrB_2–SiC ceramics. *J Eur Ceram Soc* 2007;**27**:2729–36.
5. Chamberlain AL, Fahrenholtz WG, Hilmas GE, Ellerby DT. High-strength zirconium diboride-based ceramics. *J Am Ceram Soc* 2004;**87**:1170–2.
6. Monteverde F. Beneficial effects of an ultra-fine α-SiC incorporation on the sinterability and mechanical properties of ZrB_2. *Appl Phys A* 2006;**82**:329–37.
7. Zhu SM, Fahrenholtz WG, Hilmas GE. Influence of silicon carbide particle size on the microstructure and mechanical properties of zirconium diboride-silicon carbide ceramics. *J Eur Ceram Soc* 2007;**27**:2077–83.
8. Zhu SM, Fahrenholtz WG, Hilmas GE. Enhanced densification and mechanical properties of ZrB_2–SiC processed by a preceramic polymer coating route. *Scripta Mater* 2008;**59**:123–6.
9. Chamberlain AL, Fahrenholtz WG, Hilmas GE. Low-temperature densification of zirconium diboride ceramics by reactive hot pressing. *J Am Ceram Soc* 2006;**89**:3638–45.
10. Fahrenholtz WG, Hilmas GE, Chamberlain AL, Zimmermann JW. Processing and characterization of ZrB_2-based ultra-high temperature monolithic and fibrous monolithic ceramics. *J Mater Sci* 2004;**39**:5951–7.
11. Wu WW, Zhang GJ, Kan YM, Wang PL, Vanmeensel K, Vleugels J, et al. Synthesis and microstructural features of ZrB_2–SiC-based composites by reactive spark plasma sintering and reactive hot pressing. *Scripta Mater* 2007;**57**:317–20.
12. Zhang GJ, Deng ZY, Kondo N, Yang JF, Ohji T. Reactive hot pressing of ZrB_2–SiC composites. *J Am Ceram Soc* 2000;**83**:2330–2.
13. Zhao Y, Wang LJ, Zhang GJ, Jiang W, Chen LD. Preparation and microstructure of a ZrB_2–SiC composite fabricated by the spark plasma sintering-reactive synthesis (SPS-RS) method. *J Am Ceram Soc* 2007;**90**:4040–2.
14. Zou J, Zhang G-J, Kan Y-M, Wang P-L. Pressureless densification of ZrB_2–SiC composites with vanadium carbide. *Scripta Mater* 2008;**59**:309–12.
15. Rezaie A, Fahrenholtz WG, Hilmas GE. Effect of hot pressing time and temperature on the microstructure and mechanical properties of ZrB_2–SiC. *J Mater Sci* 2007;**42**:2735–44.
16. Alida Bellosi FM, Diletta Sciti. Fast densification of ultra-high-temperature ceramics by spark plasma sintering. *Int J Appl Ceram Technol* 2006;**3**:32–40.
17. Fahrenholtz WG, Hilmas GE, Zhang SC, Zhu S. Pressureless sintering of zirconium diboride: particle size and additive effects. *J Am Ceram Soc* 2008;**91**:1398–404.

18. Vanmeensel K, Laptev A, Hennicke J, Vleugels J, Van der Biest O. Modelling of the temperature distribution during field assisted sintering. *Acta Mater* 2005;**53**:4379–88.
19. Anstis GR, Chantikul P, Lawn BR, Marshall DB. A critical evaluation of indentation techniques for measuring fracture toughness. I. Direct crack measurements. *J Am Ceram Soc* 1981;**64**:533–8.
20. Chamberlain AL, Fahrenholtz WG, Hilmas GE. Reactive hot pressing of zirconium diboride. *J Eur Ceram Soc* 2009;**29**:3401–8.
21. Radev DD, Marinov M. Properties of titanium and zirconium diborides obtained by self-propagated high-temperature synthesis. *J Alloys Compd* 1996;**244**:48–51.
22. Çamurlu HE, Maglia F. Preparation of nano-size ZrB_2 powder by self-propagating high-temperature synthesis. *J Eur Ceram Soc* 2009;**29**:1501–6.
23. Wu WW, Zhang GJ, Kan YM, Wang PL. Reactive hot pressing of ZrB_2–SiC–ZrC composites at 1600 °C. *J Am Ceram Soc* 2008;**91**:2501–8.
24. Bhosle V, Baburaj E, Miranova M, Salama K. Dehydrogenation of nanocrystalline TiH_2 and consequent consolidation to form dense Ti. *Metall Mater Trans A* 2003;**34**:2793–9.
25. Schmidt J, Niewa R, Schmidt M, Grin Y. Spark plasma sintering effect on the decomposition of MgH_2. *J Am Ceram Soc* 2005;**88**:1870–4.
26. Zhang SC, Hilmas GE, Fahrenholtz WG. Pressureless densification of zirconium diboride with boron carbide additions. *J Am Ceram Soc* 2006;**89**:1544–50.
27. Chamberlain AL, Fahrenholtz WG, Hilmas GE. Pressureless sintering of zirconium diboride. *J Am Ceram Soc* 2006;**89**:450–6.
28. Huang S, Vanmeensel K, Malek O, Van der Biest O Vleugels J, Pulsed electric current sintering of B_4C–TiB_2 composites. *J Alloys Compd*; submitted for publication.
29. Wu W-W, Wang Z, Zhang G-J, Kan Y-M, Wang P-L. ZrB_2–$MoSi_2$ composites toughened by elongated ZrB_2 grains via reactive hot pressing. *Scripta Mater* 2009;**61**:316–9.
30. Lotgering FK. Topotactical reactions with ferrimagnetic oxides having hexagonal crystal structures-I. *J Inorg Nucl Chem* 1959;**9**:113–23.
31. Ni D-W, Zhang G-J, Kan Y-M, Sakka Y. Highly textured ZrB_2-based ultra-high temperature ceramics via strong magnetic field alignment. *Scripta Mater* 2009;**60**:615–8.
32. Seabaugh MM, Kerscht IH, Messing GL. Texture development by templated grain growth in liquid-phase-sintered α-alumina. *J Am Ceram Soc* 1997;**80**:1181–8.
33. Shen Z, Zhao Z, Peng H, Nygren M. Formation of tough interlocking microstructures in silicon nitride ceramics by dynamic ripening. *Nature* 2002;**417**:266–9.
34. Jensen MS, Einarsrud M-A, Grande T. Preferential grain orientation in hot pressed TiB_2. *J Am Ceram Soc* 2007;**90**:1339–41.
35. Ran S, Zhang L, Van der Biest O, Vleugels J. Pulsed electric current, in situ synthesis and sintering of textured TiB_2 ceramics. *J Eur Ceram Soc* 2010;**30**:1043–7.
36. Wurst JC, Nelson JA. Linear intercept technique for measuring grain size in two-phase polycrystalline ceramics. *J Am Ceram Soc* 1972;**55**:109–109.
37. Guo S-Q, Kagawa Y, Nishimura T, Chung D, Yang J-M. Mechanical and physical behavior of spark plasma sintered ZrC–ZrB_2–SiC composites. *J Eur Ceram Soc* 2008;**28**:1279–85.